



Few-cycle 65- μJ pulses at 11.4 μm for ultrafast nonlinear longwave-infrared spectroscopy

PIA FUERTJES,  MARTIN BOCK, LORENZ VON GRAFENSTEIN, DENNIS UEBERSCHAER, UWE GRIEBNER,* AND THOMAS ELSAESSER

Max Born Institute for Nonlinear Optics and Short Pulse Spectroscopy, Max-Born-Str. 2a, D-12489 Berlin, Germany

*Corresponding author: griebner@mbi-berlin.de

Received 8 August 2022; revised 13 October 2022; accepted 13 October 2022; published 18 November 2022

Low-energy excitations can provide insight into the basic ultrafast nonequilibrium dynamics of condensed matter. High-energy femtosecond pulses in the long-wavelength infrared are required to induce such processes, and can be generated in an optical parametric chirped pulse amplification (OPCPA) system comprising three GaSe stages. A femtosecond Cr:ZnS laser serves as the front-end, providing the seed for the 2.0- μm pump and the 2.4- μm signal pulses without nonlinear conversion processes. The OPCPA system is pumped at 2.05 μm by a picosecond Ho:YLF regenerative amplifier at a 1-kHz repetition rate. The recompressed idler pulses at 11.4 μm have a duration of 185 fs and an unprecedented energy of 65 μJ , corresponding to a pump-to-idler conversion efficiency of 1.2%. Nonlinear transmission experiments in the range of the L2 infrared band of liquid water demonstrate the potential of the pulses for nonlinear vibrational spectroscopy of liquids and solids. © 2022 Optica Publishing Group under the terms of the Optica Open Access Publishing Agreement

<https://doi.org/10.1364/OPTICA.472650>

The generation of ultrashort pulses in the long-wave infrared (LWIR) at wavelengths between 6 and 20 μm has attracted much attention because of their strong application potential in basic research [1]. In this context, nonlinear femtosecond infrared spectroscopy of intra- and intermolecular low-frequency vibrations is an important research area, which requires intense broadband pulses because of the comparably small transition dipoles and broad complex line shapes. Moreover, long-wavelength pulses with peak optical fields beyond 1 megavolt/cm (MV/cm) provide access to nonperturbative light–matter interactions and field-driven processes in condensed matter [2–5].

Broadband LWIR pulses have been generated by nonlinear frequency downconversion in difference frequency generation (DFG) or optical parametric amplifier (OPA) arrangements [6–11]. Generating high-energy femtosecond pulses at wavelengths beyond 10 μm and kHz repetition rates has remained a major technological challenge, due to the limited availability and optical transparency of nonlinear crystals [12]. Beyond 10 μm , pulse energies of the order of 1 μJ with a sub-200 fs pulse duration have been demonstrated with HgGa₂S₄ and AgGaS₂ [6], AgGaSe₂ [13], and GaSe [7,9,10] nonlinear crystals. Only very recently, pulse

energies of up to 17 μJ beyond 10 μm were achieved via DFG in GaSe [13,14].

A key technique for scaling the energy of mid-IR ultrashort pulses at kHz repetition rates even higher is optical parametric chirped pulse amplification (OPCPA) [15,16]. With high-performance Ho-doped 2- μm pump sources, millijoule-range femtosecond OPCPA systems were reported for the 5 to 7 μm range [15–17], all based on ZnGeP₂ crystals. For the LWIR range, such OPCPA systems have been modeled theoretically but lack experimental implementation [18]. A challenge for the practical implementation of mid-IR OPCPA systems is their, in general, complex front-end architecture. Seed pulses for pump and signal are typically generated by multi-stage nonlinear processes [15,16], which affects both efficiency and stability.

Among the nonlinear crystals for the LWIR range, GaSe stands out with its high second order nonlinearity ($d_{\text{eff}} = 54 \text{ pm/V}$) and comparatively high damage threshold [13,19–21]. Employing a pump wavelength of 2 μm is advantageous compared to drivers at shorter near-infrared wavelengths [6–11] when aiming at energy scaling of the idler pulses [20,21]. The bandgap of GaSe is at 2.1 eV ($\lambda = 0.59 \mu\text{m}$), resulting in strong two-photon absorption of pump pulses at wavelengths shorter than 1.2 μm . Due to the expected higher crystal damage threshold, higher intensities when pumping at 2 μm instead of 1 μm are possible and, furthermore, 2- μm pumping offers a higher pump-to-idler conversion efficiency.

Here, we report a table-top LWIR OPCPA system with a femtosecond Cr:ZnS oscillator acting as the front-end without additional nonlinear stages. Pumped at 2.0 μm , the system has three GaSe amplification stages with nonlinear crystals of different thicknesses. The 2.0- μm seed pulses are amplified to 13 mJ in a picosecond Ho:YLF regenerative amplifier (RA). Parametric amplification provides idler pulses centered at 11.4 μm , with an unprecedented pulse energy of $\sim 70 \mu\text{J}$ at a 1-kHz repetition rate. Recompression results in few-cycle pulses of a sub-200 fs duration and 0.35-GW peak power, allowing for peak optical fields of several tens of MVs/cm in the focused output beam. We demonstrate the potential of this source for ultrafast infrared spectroscopy in nonlinear transmission experiments with liquid water.

The experimental scheme of the LWIR OPCPA system is shown in Fig. 1(a). The front-end consists of a mode-locked Cr:ZnS oscillator operating at a repetition rate of 79 MHz (IPG Photonics). Its output spectrum is centered at 2.4 μm and extends

from 1.95–2.55 μm ($1/e^2$ level). The pulses have a duration and energy of 30 fs and 12.5 nJ, respectively. Without any nonlinear frequency conversion, the Cr:ZnS emission spectrum directly provides the seed for the pump at 2.0 μm and for the signal at 2.4 μm . A dichroic mirror placed at the output of the Cr:ZnS laser separates the spectrum into two parts below and above 2.1 μm . The splitting of the spectrum has little impact on the duration of the remaining signal pulses centered at 2.4 μm with a pulse duration of 46 fs and 10-nJ energy [17].

The 2- μm pump source has been presented in detail in [17]. Prior to amplification, the seed pulse is stretched to ~ 1 ns by a chirped volume Bragg grating that reflects the spectral window from 2045 to 2055 nm. After pre-amplification in a Tm:fiber amplifier, the pulses are coupled into a Ho:YLF RA, pumped by a continuous-wave Tm:fiber laser. Seeding the RA with ~ 2.5 nJ, the pulses are amplified to 13 mJ in a 1-kHz pulse train. The final compression provides 3-ps pulses with 12-mJ energy at 2.05 μm , serving as pump for the OPCPA stages.

The signal seed pulses from the Cr:ZnS oscillator are first temporally stretched in a 40-mm-long antireflection (AR) coated sapphire rod. The negatively chirped pulses are then subject to phase shaping by an acousto-optic programmable dispersive filter (Dazzler, Fastlite), which is accompanied by 90% loss of pulse energy. The resulting pulse duration amounts to ~ 1.5 ps. The OPCPA chain consists of three GaSe amplification stages. The aperture of the GaSe crystals with a diameter of 7 mm is identical in the three stages.

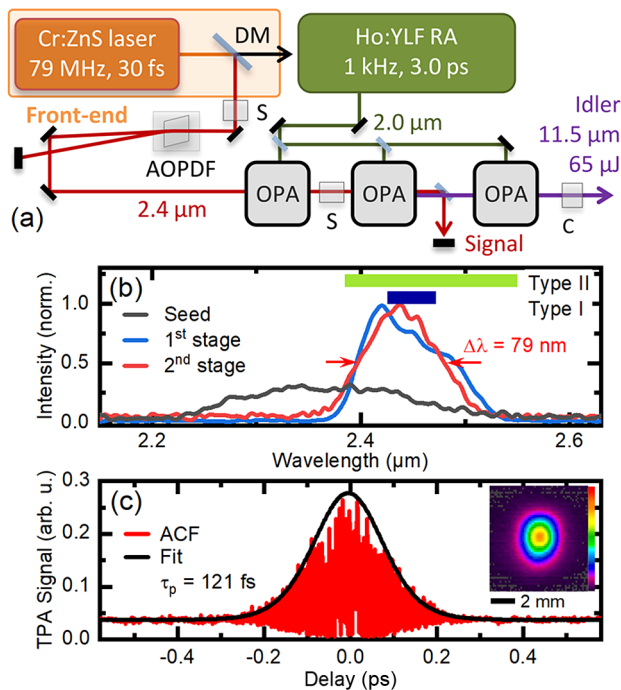


Fig. 1. (a) Setup of the LWIR OPCPA system. The main parts are the front-end with the fs Cr:ZnS master oscillator, the Ho:YLF regenerative amplifier (RA) as pump, and the three optical parametric amplifier (OPA) stages based on GaSe crystals. AOPDF, acousto-optic programmable dispersive filter; S, bulk stretcher; C, compressor; DM, dichroic mirror. (b) Characterization of the GaSe-based OPCPA signal pulses. Seed spectrum (black line), signal spectrum after the first (blue line) and second OPA stages (red line). The green and blue bars indicate the bandwidth (FWHM) of type I and type II phase matching for GaSe for the 2.05- μm pump, respectively. (c) Collinear autocorrelation function (ACF) of the compressed signal pulse after the second stage; inset: far-field intensity distribution.

The phase-matching bandwidth for the signal was calculated from the GaSe dispersion data for type I and type II phase matching [Fig. 1(b)]. Type II phase matching supports a broader bandwidth and is, thus, selected for our OPCPA system. In all stages, the parametric process is phase matched at an internal angle of 12.2° corresponding to an external angle of 36° . Since there is no AR coating on the GaSe crystals, 16% of the p -polarized pump and 27% of the s -polarized signal are reflected at each surface.

Pumping the 2-mm-thick GaSe crystal in the first collinear stage with 0.3 mJ, the signal pulses are amplified to 13 μJ . The pump intensity is chosen slightly below $50 \text{ GW}/\text{cm}^2$ in all stages, limited by the damage threshold of GaSe [13,20,21]. A small angle of $<0.5^\circ$ between the pump and the signal is introduced (much less than in non-collinear phase matching) to prevent the second stage from being seeded with the second harmonic of the pump from the first stage. The latter process is not phase matched and very inefficient. The spectra of the signal and idler pulses are measured applying a scanning monochromator (Horiba). Due to the phase matching conditions, the signal pulses are redshifted relative to the spectrum of the seed pulses [Fig. 1(b), black curve] and have a spectral width of 97 nm (FWHM) [Fig. 1(b), blue curve], limited by the phase matching bandwidth. The signal pulses are shortened in the parametric amplification process and, thus, need to be stretched again in time to adapt the signal and pump pulse durations in the following parametric amplifier stages. This is performed in a 90-mm-long AR-coated sapphire rod and results in a signal pulse duration of 1.9 ps.

In the second collinear parametric amplification stage, we use a 1-mm-thick GaSe crystal and a pump energy of 1.8 mJ. After amplification, the combined signal and idler energy in the 1-kHz pulse train has a value of 148 μJ (128- μJ signal, 20- μJ idler). The measured signal spectrum is centered at 2.44 μm with a bandwidth of 79 nm [Fig. 1(b), red curve] indicating a limited saturation of parametric amplification, which we confirmed by simulations based on the numerical code Sisyfos.

The corresponding idler pulses are centered at 11.4 μm with a FWHM of 0.84 μm [Fig. 2(a)], supporting a pulse duration of 170 fs. The measured idler energy reaches a high value of 20 μJ at this stage already. To demonstrate the compressibility of the amplified signal pulses, a Martinez-type compressor in a $4-f$ -setup based on sapphire prisms was installed. The measured interferometric autocorrelation trace (miniTPA, APE) of the compressed signal pulses is presented in Fig. 1(c). Assuming a sech^2 -pulse shape, a duration of 124 fs is extracted from this trace, which is close to the Fourier-transform limit (FTL). The energy throughput of the compressor is $\sim 50\%$, limited mostly by Fresnel losses at the uncoated lenses. The output beam profile recorded with a Pyrocam camera (Ophir) is nearly Gaussian and shown in the inset of Fig. 1(c).

The third stage is equipped with a 1-mm-thick GaSe crystal and seeded with the idler pulse only [Fig. 1(a)]. Due to the limited aperture of the GaSe crystal, only 4.2 mJ of the total remaining pump energy of 10 mJ can be utilized in this booster stage to prevent damage of GaSe. The idler seed pulse has to be shaped for the best spatial beam overlap with the pump using two additional lenses, which reduces its energy to 8 μJ . The third amplification stage enhances the idler pulse energy to its final value of 73 μJ , a record number for sub-picosecond pulses beyond 10 μm [13,14]. The resulting pump-to-idler energy overall conversion efficiency

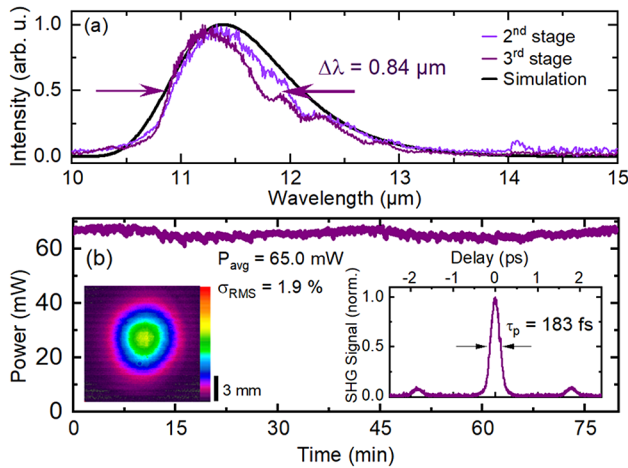


Fig. 2. Characterization of the GaSe-based OPCPA idler pulse performance. (a) Measured spectra after the second (violet) and third OPA stages (magenta) and calculated spectrum based on the signal spectrum after the second stage (blue); (b) long-term pulse stability measurement of the re-compressed pulses. Left inset: far-field intensity distribution after the third stage. Right inset: ACF of the re-compressed pulse after the third stage.

amounts to a remarkable 1.2%, and the average power in the 1-kHz pulse train has a value of 73 mW.

The idler spectrum after the third amplification stage is almost unchanged compared to that after the second stage [Fig. 2(a), magenta curve]. Both spectra are close to the simulated idler spectrum [Fig. 2(a), violet curve]. The experimental idler spectra exhibit slight spectral modulations, which we attribute to a weak interference of the main and a residual idler beam, the latter originating from reflections at the uncoated surfaces of the GaSe crystal.

AR-coated ZnSe windows of 5-mm thickness are used for re-compression of the positively chirped idler pulses of 0.8-ps duration. This bulk compressor consists of two lenses and two ZnSe windows causing a loss of 10%. The energy of the compressed idler pulses amounts to 65 μ J [Fig. 2(b)]. The beam profile is nearly diffraction limited [left inset, Fig. 2(b)] with a remarkable stability of the recompressed pulses (rms: < 2%). The latter is confirmed by the long-term power measurement shown in Fig. 2(b).

Fine tuning of the dispersion was performed by the acousto-optic programmable dispersive filter (AOPDF). The duration of the compressed pulses is first measured at a long time scale with a homemade non-collinear autocorrelator (AC) where a 0.1-mm-thick GaSe serves as the second-harmonic generation (SHG) crystal and the Pyrocam as the detector exhibiting a 1000:1 linear dynamic range. The result is shown in the right inset of Fig. 2(b) and indicates a pulse duration of 183 fs assuming a Gaussian pulse shape. The accompanying weak satellites at a delay of ± 1.8 ps are caused by reflections in the 0.1-mm-thick SHG crystal, i.e., they are measurement artifacts.

For a phase-resolved characterization of the idler pulses, the Pyrocam camera was replaced by the scanning monochromator in the AC setup to record a SHG frequency-resolved optical gating (FROG) trace with a spectral resolution of 10 nm (Fig. 3). The measured FROG trace [Fig. 3(a)] shows a regular modulation on the spectrum, which is again due to the uncoated 0.1-mm-thick SHG crystal, i.e., not to a modulation on the incoming idler pulse. This modulation was suppressed in the pulse retrieval and, thus, is

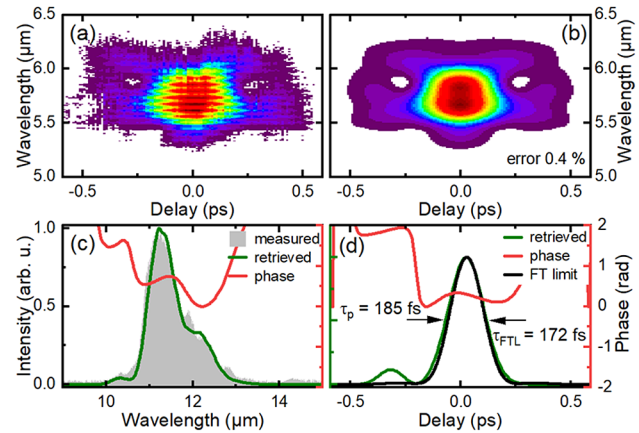


Fig. 3. SHG-FROG characterization of the idler pulses after the third OPA stage. (a), (b) SHG-FROG trace measured and retrieved; (c) optical spectrum, measured (gray), retrieved (green), and phase (red); (d) retrieved temporal pulse shape. FTL, Fourier-transform limit.

not visible there [Fig. 3(b)]. The spectral phase is flat, confirming the good pulse quality [Fig. 3(c), red line].

The retrieved pulse shape yields a pulse duration of 185 fs (FWHM) [Fig. 3(d)]. It deviates by only 7% from the FTL limit and corresponds to less than five optical cycles. The FROG error amounts to 0.4%. Taking into account the 65- μ J pulse energy, one derives a peak power of 0.35 GW, translating into a peak intensity of 4.45 TW/cm² in a focused beam of 100- μ m diameter and a peak optical field of some 40 MV/cm. These values surpass those reported for femtosecond DFG or OPA's beyond 10 μ m by far [9,13,14].

Nonlinear transmission experiments with neat liquid water were performed to demonstrate the potential of our novel source for ultrafast vibrational spectroscopy. The spectrum of the 11.4- μ m pulses fully overlaps with the broad librational (L2) absorption band of water [black line in Fig. 4(a)], showing a maximum at 14.9 μ m (670 cm⁻¹), an asymmetric spectral envelope of a width (FWHM) of 460 cm⁻¹, and a peak molar extinction coefficient of $\epsilon = 30$ M⁻¹ cm⁻¹ [22,23]. The underlying molecular excitations are hindered rotations of water molecules around the axis with the lowest moment of inertia. So far, the nonlinear response connected with such librational excitations has remained unexplored, and the infrared line shape is not understood.

In the experiments, the compressed idler pulses were focused to a beam diameter of 130 μ m resulting in a peak intensity of 1.0 TW/cm² for a pulse energy of 25 μ J. The transmission of a 12- μ m-thick H₂O film, held between two 1-mm-thick BaF₂ windows was recorded as a function of pulse energy, using the Pyrocam camera [Fig. 4(b)]. At each point, the transmission was measured in parallel for an identical cell without water (air-filled) to eliminate the influence of the BaF₂ windows on the transmission change.

The spectra of the incident and transmitted pulses (incident pulse energy 25 μ J) are presented in Fig. 4(a). The stronger absorption at low frequencies leads to a reduction of low-frequency components in the transmitted spectrum, while any broadening due to self-phase modulation is absent. We observe a nonlinear transmission increase of 1.4% [Fig. 4(b)], which points to a bleaching of the original librational $\nu = 0$ ground state. This mechanism is similar to the nonlinear response of the OH bend and stretch vibrations of water, but different from high-frequency librations

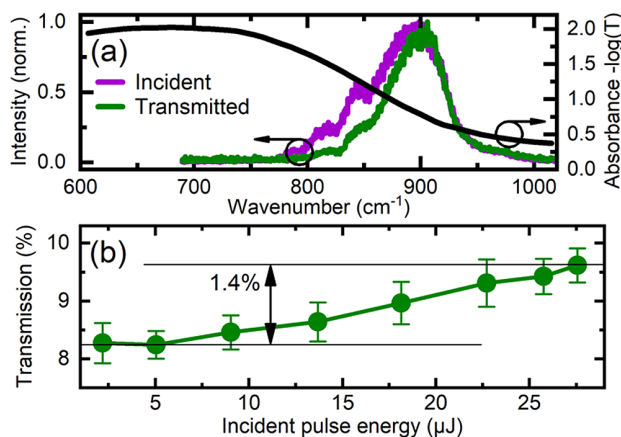


Fig. 4. Nonlinear transmission of liquid H_2O at the librational (L2) band. (a) L2 absorption of water (black, sample thickness $12\ \mu\text{m}$) and incident (magenta) and transmitted (green) spectra of the $11.4\text{-}\mu\text{m}$ pulses (energy $25\ \mu\text{J}$). (b) Transmission of the water sample as a function of incident pulse energy, showing a nonlinear transmission increase.

around $1350\ \text{cm}^{-1}$, the latter showing an initial transmission decrease [24].

For an incident pulse energy of $25\ \mu\text{J}$, some 20% of the water molecules in the interacting sample volume are excited. This would result in a transmission change of several 10% if the lifetime of the L2 excitation was significantly longer than the pulse duration (time-integrating behavior). The much smaller transmission change observed here points to a sub-50-fs librational lifetime, which will be explored in detail in future time-resolved experiments.

In conclusion, we have demonstrated a compact multi-stage OPCPA working at a 1-kHz repetition rate and providing LWIR pulses at a center wavelength of $11.4\ \mu\text{m}$ with a pulse duration of 185 fs. The OPCPA consists of three GaSe stages pumped at $2\ \mu\text{m}$ by picosecond pulses from a Ho:YLF RA. The record output pulse energy of $65\ \mu\text{J}$ at $11.4\ \mu\text{m}$ translates to a peak power of 0.35 GW and peak intensities of several TW/cm^2 in the focused output beam. Even higher idler pulse energies may be generated in novel nonlinear crystals for this spectral range, such as BGSe and BGGSe₂ [25]. Experiments with liquid water demonstrate the potential of this source for nonlinear vibrational spectroscopy and studies of non-perturbative light–matter interactions.

Funding. Deutsche Forschungsgemeinschaft (GR2115/6-1); Horizon 2020 Framework Programme (871124).

Disclosures. The authors declare no conflicts of interest.

Data availability. Data underlying the results presented in this paper are not publicly available at this time but may be obtained from the authors upon reasonable request.

REFERENCES

- H. Pires, M. Baudisch, D. Sanchez, M. Hemmer, and J. Biegert, *Prog. Quantum Electron.* **43**, 1 (2015).
- F. Dahms, B. P. Fingerhut, E. T. J. Nibbering, E. Pines, and T. Elsaesser, *Science* **357**, 491 (2017).
- A. Ghalgaoui, L.-M. Koll, B. Schütte, B. P. Fingerhut, K. Reimann, M. Woerner, and T. Elsaesser, *J. Phys. Chem. Lett.* **11**, 7717 (2020).
- M. Wagner, A. S. McLeod, S. J. Maddox, Z. Fei, M. Liu, R. D. Averitt, M. M. Fogler, S. R. Bank, F. Keilmann, and D. N. Basov, *Nano Lett.* **14**, 4529 (2014).
- G. P. Szekeres, K. Pagel, and Z. Heiner, *Anal. Bioanal. Chem.* **414**, 85 (2021).
- F. Rotermund, V. Petrov, and F. Noack, *Opt. Commun.* **185**, 177 (2000).
- F. Junginger, A. Sell, O. Schubert, B. Mayer, D. Brida, M. Marangoni, G. Cerullo, A. Leitenstorfer, and R. Huber, *Opt. Lett.* **35**, 2645 (2010).
- D. J. Wilson, A. M. Summers, S. Zigo, B. Davis, S.-J. Robotjazi, J. A. Powell, D. Rolles, A. Rudenko, and C. A. Trallero-Herrero, *Sci. Rep.* **9**, 6002 (2019).
- M. Babzien, I. V. Pogorelsky, and M. Polanskiy, *AIP Conf. Proc.* **1777**, 110001 (2016).
- K. Liu, H. Liang, L. Wang, S. Qu, T. Lang, H. Li, Q. J. Wang, and Y. Zhang, *Opt. Lett.* **44**, 1003 (2019).
- Z. Heiner, V. Petrov, V. L. Panyutin, V. V. Badikov, K. Kato, K. Miyata, and M. Mero, *Sci. Rep.* **12**, 5082 (2022).
- V. Petrov, *Prog. Quantum Electron.* **42**, 1 (2015).
- M. Duda, L. von Grafenstein, M. Bock, D. Ueberschaer, P. Fuertjes, L. Roškot, M. Smrž, O. Novák, and U. Griebner, *Opt. Lett.* **47**, 2891 (2022).
- R. Budriunas, K. Jurkus, M. Vengris, and A. Varanavicius, *Opt. Express* **30**, 13009 (2022).
- L. von Grafenstein, M. Bock, D. Ueberschaer, E. Escoto, A. Koç, K. Zawilski, P. Schunemann, U. Griebner, and T. Elsaesser, *Opt. Lett.* **45**, 5998 (2020).
- U. Elu, T. Steinle, D. Sánchez, L. Maidment, K. Zawilski, P. Schunemann, U. D. Zeitner, C. Simon-Boisson, and J. Biegert, *Opt. Lett.* **44**, 3194 (2019).
- P. Fuertjes, L. von Grafenstein, D. Ueberschaer, C. Mei, U. Griebner, and T. Elsaesser, *Opt. Lett.* **46**, 1704 (2021).
- A. A. Voronin, A. A. Lanin, and A. M. Zheltikov, *Opt. Express* **24**, 23207 (2016).
- K. L. Vodopyanov, L. A. Kulevskii, V. G. Voevodin, A. I. Gribenyukov, K. R. Allakhverdiev, and T. A. Kerimov, *Opt. Commun.* **83**, 322 (1991).
- T. P. Butler, D. Gerz, C. Hofer, J. Xu, C. Gaida, T. Heuermann, M. Gebhardt, L. Vamos, W. Schweinberger, J. A. Gessner, T. Siefke, M. Heusinger, U. Zeitner, A. Apolonski, N. Karpowicz, J. Limpert, F. Krausz, and I. Pupeza, *Opt. Lett.* **44**, 1730 (2019).
- Q. Cao, F. X. Kärtner, and G. Chang, *Opt. Express* **28**, 1369 (2020).
- H. R. Zelsmann, *J. Mol. Struct.* **350**, 95 (1995).
- J. E. Bertie and Z. Lan, *Appl. Spectrosc.* **50**, 1047 (1996).
- N. Huse, S. Ashihara, E. T. J. Nibbering, and T. Elsaesser, *Chem. Phys. Lett.* **404**, 389 (2005).
- V. Petrov, V. V. Badikov, D. V. Badikov, K. Kato, G. S. Shevyrdyaeva, K. Miyata, M. Mero, L. Wang, Z. Heiner, and V. L. Panyutin, *J. Opt. Soc. Am. B* **38**, B46 (2021).